An Assessment of Errors in the Simulation of Atmospheric Interannual Variability in Uncoupled AGCM Simulations

ARUN KUMAR

NOAA/Climate Prediction Center, Camp Springs, Maryland

QIN ZHANG

RSIS Climate Prediction Center, Camp Springs, Maryland

J.-K. E. SCHEMM AND MICHELLE L'HEUREUX

NOAA/Climate Prediction Center, Camp Springs, Maryland

K.-H. SEO

Pusan National University, Busan, South Korea

(Manuscript received 24 October 2006, in final form 6 August 2007)

ABSTRACT

For the uncoupled atmospheric general circulation model (AGCM) simulations, the quantification of errors due to the lack of coupled ocean–atmospheric evolution on the characteristics of the atmospheric interannual variability is important for various reasons including the following: 1) AGCM simulations forced with specified SSTs continue to be used for understanding atmospheric interannual variability and 2) there is a vast knowledge base quantifying the global atmospheric influence of tropical SSTs that traditionally has relied on the analysis of AGCM-alone simulations. To put such results and analysis in a proper context, it is essential to document errors that may result from the lack of a coupled ocean–atmosphere evolution in the AGCM-alone integrations.

Analysis is based on comparison of tier-two (or uncoupled) and coupled hindcasts for the 1982–2005 period, and interannual variability for the December–February (DJF) seasonal mean is analyzed. Results indicate that for the seasonal mean variability, and for the DJF seasonal mean, atmospheric interannual variability between coupled and uncoupled simulations is similar. This conclusion is drawn from the analysis of interannual variability of rainfall and 200-mb heights and includes analysis of SST-forced interannual variability, analysis of El Niño and La Niña composites, and a comparison of hindcast skill between tier-two and coupled hindcasts.

1. Introduction

The focus of this paper is to assess the influence of the lack of coupled ocean–atmospheric evolution on the atmospheric mean state and its interannual variability in the *atmosphere-alone* general circulation model simulations. Atmospheric general circulation model (AGCM) simulations forced with observed sea surface temperatures (SSTs), the so-called Atmospheric Model Intercomparison Project (AMIP) integrations (Gates 1992), have been extensively used for attributing, understanding, and documenting atmospheric interannual variability (Lau 1997; Trenberth et al. 1998; Hoerling and Kumar 2002). Continued use of AMIP simulations as a tool for understanding this variability is evident from a quick survey of recent literature (Biasutti et al. 2006; Nigam and Ruiz-Barradas 2006; Nakaegawa and Kanamitsu 2006; Kharin et al. 2005; Annamalai et al. 2005). Notwithstanding the popularity of AMIP simulations as an analysis tool, it has also been well established that certain facets of observed reality are misrep-

Corresponding author address: Dr. Arun Kumar, Climate Prediction Center, NOAA/NWS/NCEP, 5200 Auth Road, Rm. 800, Camp Springs, MD 20746.
E-mail: arun.kumar@noaa.gov

DOI: 10.1175/2007JCLI1743.1

resented in the AMIP simulations. Most notable is the missing influence of air–sea interactions on the evolution of ocean characteristics, for example, sea surface temperature (Gallimore 1995; Barsugli and Battisti 1998; Bretherton and Battisti 2000). This is because in the AMIP simulations SST is *specified* and its time history is not consistent with the surface momentum and heat fluxes. A question is to what extent inferences about atmospheric interannual variability based on AMIP simulations are erroneous owing to such approximations. This question is assessed based on a comparison of coupled and atmosphere-alone model integrations.

Although differences due to inclusion or neglect of coupled ocean–atmosphere evolution could be studied on variety of different time scales, the focus of this study is on the simulation of the atmospheric mean state and interannual variability of seasonal means. This particular focus stems from the fact that a long history of analysis aided by the AMIP simulations has led to appreciable understanding of the influence of tropical SSTs on the global atmospheric circulation (Trenberth et al. 1998; Hoerling and Kumar 2002). Therefore it is desirable to validate our current knowledge of the global influence of tropical SSTs in the context that this understanding may be erroneous because of approximating the coupled ocean–atmosphere system in the AMIP simulations.

To understand the influence of the coupled ocean–atmosphere evolution on the characteristics of atmospheric variability, integrations from a coupled general circulation model (CGCM) and its AGCM counterpart are compared. The time history (or the interannual variability) of SSTs is kept the same in the CGCM and AGCM integrations by specifying the interannual variability of SSTs in the AGCM integrations from the corresponding CGCM integrations: therefore, differences in atmospheric interannual variability between two sets of integrations point to the possible influence of coupled ocean–atmosphere evolution.

The coupled and the uncoupled general circulation model simulations are described in section 2. Analysis of the atmospheric mean state and interannual variability of seasonal means is described in section 3. Concluding remarks on the extent of the influence of coupled ocean–atmosphere evolution on the atmospheric variability are presented in section 4.

2. Data and model simulations

An extensive set of hindcasts were completed with the current operational Climate Forecast System (CFS) at the National Centers for Environmental Prediction (NCEP; Saha et al. 2006; Wang et al. 2005). In the coupled hindcast integrations, due to errors in the CGCM, predicted SSTs are generally biased. If the SST bias in coupled predictions is large and even SST anomalies are predicted correctly, then it is possible that biases in the mean state may adversely influence prediction of atmospheric interannual variability. For this reason, when the dynamical seasonal prediction methods first evolved, a routine practice was to bias correct the predicted SST anomalies and then use the bias-corrected SSTs to rerun AGCM-alone integrations to generate predictions for the atmospheric anomalies (Bengtsson et al. 1993; Ji et al. 1994). This procedure for generating dynamical seasonal forecasts is generally referred to as a two-tiered prediction system.

Following the two-tiered prediction approach described above, NCEP created a set of hindcast experiments using the bias-corrected SSTs predicted by the coupled CFS hindcast. As for the two-tiered prediction system, the purpose of this additional set of experiments was to assess if further improvement in the prediction skill may result from the bias correction of predicted SSTs. Availability of these two sets of hindcasts, however, also allows us to glean some insight into the question of misrepresentation of coupled ocean–atmosphere evolution on the atmospheric mean state and the interannual variability of seasonal means in the AGCM-alone integrations. Details of the experimental setup for the hindcasts are outlined next.

The coupled CFS hindcasts are done for 1982–2005, and there are 15 forecast integrations for each forecast month in that period. These forecasts are clustered around the 1st, 11th, and 21st of the month. For example, for the month of January 1982, there are five forecasts, each initialized from the observed atmospheric initial conditions centered on 1, 11, and 21 January. Furthermore, for each cluster of five forecasts, ocean initial states are obtained from the NCEP Global Ocean Data Assimilation System (GODAS). Forecast integrations are for 10 months from the date of initialization.

Once the coupled CFS hindcasts for the entire period are available, the monthly mean bias in predicted SST is obtained by comparing them with the observed SSTs. The SST bias depends on the lead time of the forecast. For example, the bias for the month of January depends on whether the forecasts are initialized from the month of December or from the month of November.

For the tier-two hindcast experiments, monthly SST bias for each forecast month from the CFS hindcast is removed. Bias correction for monthly mean SSTs is preferred as a bias correction procedure for daily fields is not feasible because of the shortness of data and

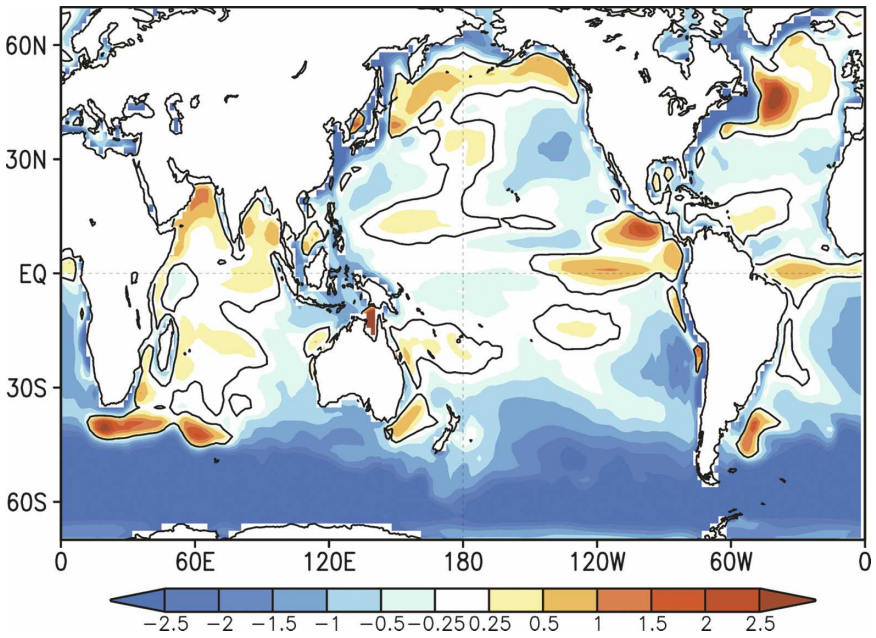

FIG. 1. Observed minus coupled model hindcast SST climatology for the DJF seasonal mean. Climatology was computed based on the 1982–2005 period, and a 15-member ensemble mean was used for the model. Units are in °C and the zero contour is plotted.

problems with estimating daily climatology. The bias-corrected monthly SSTs are then used to force the atmospheric component of the CFS, and the hindcasts for initial conditions for the selected months are repeated for the entire forecast period. For these hindcasts, an ensemble of 15 forecast integrations is also used. The bias correction procedure is such that it maintains the interannual variability of predicted SSTs.

In the present experimental setup, differences between the coupled and tier-two hindcasts, therefore, are 1) the mean state of SST itself differs although the interannual variability of the SSTs between coupled and tier-two hindcast runs is the same and 2), while the evolution of the ocean state in the coupled hindcasts is consistent with the momentum and heat fluxes across the ocean–atmosphere interface, such consistency does not exist in tier-two integrations. The experimental setup, therefore, is not ideal to analyze the question of the influence of the lack of coupled ocean–atmosphere evolution on the atmospheric interannual variability. However, given that the bias in the CGCM-predicted tropical SSTs are generally small, a comparison of atmospheric variability between two sets of hindcasts can still be used to obtain some insights about the question we posed.

The tier-two hindcasts experiments have been repeated for initial conditions for four different months: April, July, October, and January. The analysis reported in this paper, however, is for the December–February (DJF) seasonal mean hindcasts from the initial conditions from the month of October. This season was chosen because of the extensive array of AMIP-based studies that have analyzed the characteristics of the global atmospheric response to SST variability in tropical and extratropical oceans (Lau 1997; Hoerling and Kumar 2002). To complement the analysis for the winter season, an analysis for the summer season of June–September (JJAS) from the April initial conditions was also done. All model analyses are for the 15-member ensemble.

DJF hindcasts from coupled and tier-two experiments are also verified against the observed seasonal means. For verifications, the observed 200-mb seasonal mean heights are obtained from the NCEP–NCAR reanalysis. The observed seasonal mean rainfall is obtained from the Climate Anomaly Monitoring System–Outgoing Longwave Radiation (OLR) Precipitation Index (CAMS–OPI) rainfall estimates (Janowiak and Xie 1999). Observed and model anomalies for each variable are computed from their respective 1982–2005 DJF climatology.

3. Results

a. Analysis of differences in the mean state

Shown in Fig. 1 is the bias in the CFS SST forecasts for DJF. The bias is computed by a difference between the observed and the CFS-predicted SST climatology

averaged over the 1982–2005 period.[1] In general, the observed SSTs are cooler than the CFS-predicted SSTs. Largest bias in the predicted SSTs are located in a zonal band in the Southern Hemisphere south of 45°S and off the western coast of continental regions that in the observations are associated with the persistent stratus cloud decks. These errors, therefore, are due to inadequate cloudiness in the CFS predictions resulting in too large shortwave insolation at the ocean surface (not shown). In the tropical equatorial Pacific, however, the absolute value of SST bias in CFS prediction is generally less than 0.5°C (except over the Maritime Continent and in the cold tongue of equatorial tropical eastern Pacific).

The rainfall bias over the oceanic regions for the coupled and tier-two hindcast runs is compared in Fig. 2. The largest difference in rainfall bias between the coupled and the tier-two hindcasts is around the Maritime Continent with tier-two hindcasts having a much larger drier bias than for the coupled hindcasts. Otherwise, the spatial pattern of rainfall bias between the two hindcasts is similar, with a spatial correlation between the two maps being 0.65.

Smaller rainfall bias over the Maritime Continent for the coupled hindcast is due to oceanic adjustments to errors in surface heat fluxes. For the AMIP simulations we know that rainfall over this region is negatively biased (Fig. 2, middle panel); negative rainfall bias leads to increased shortwave insolation at the ocean surface and results in an increase in local SST; increased local SSTs in turn lead to larger rainfall relative to the AMIP simulation. Therefore, because of the oceanic adjustment, although the SSTs in the coupled hindcasts stabilize toward a (biased) warm state, the corresponding rainfall has less bias compared to the AMIP hindcast.

Spatial characteristics of differences in rainfall climatology between coupled and the two-tier hindcasts (Fig. 2, bottom panel) are similar to the SST bias in the coupled run shown in Fig. 1. For example, wherever coupled hindcast SST is biased warmer (cooler), the rainfall tends to be larger (smaller) than in the tier-two hindcasts [where bias in SST was corrected, and owing to the removal of warm (cold) bias, the mean SSTs are cooler (warmer)]. This is true over equatorial regions of the Atlantic, eastern tropical Pacific, and the Indian Ocean where SST climatology in the coupled hindcasts was cooler than the observed. To substantiate this further, a scatterplot of the differences in SSTs and rainfall between two sets of hindcasts is shown in Fig. 3, and indicates that the differences in the mean rainfall, indeed tend to coincide with the differences in the mean SST state. The scatterplot also shows the classic nonlinear dependence of rainfall on mean SSTs; when the warmer bias from the SST is removed, the differences in rainfall anomalies tend to asymptote to a constant value (see lower-left quadrant in Fig. 3), a feature that is similar for the tropical rainfall response to increasing La Niña SST anomalies (Hoerling and Kumar 2002).

Although in the tropical latitudes, differences in the mean rainfall in general follow differences in mean

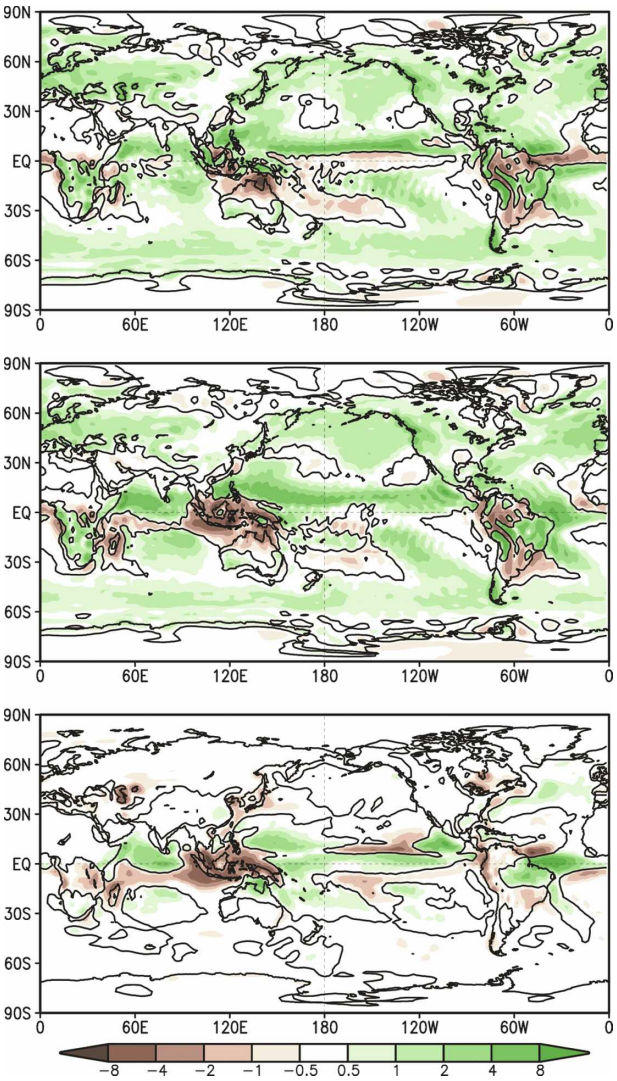

FIG. 2. Model minus observed DJF seasonal-mean rainfall climatology for the (top) coupled model and (middle) tier-two hindcast. (bottom) The tier-two minus coupled hindcast rainfall climatology for DJF seasonal mean. Climatology was computed based on the 1982–2005 period, and a 15-member ensemble mean was used for the model. Units are mm day^{-1} and the zero contour is plotted.

[1] To facilitate comparison with subsequent analysis, bias is shown as difference between the observed and the CFS predictions.

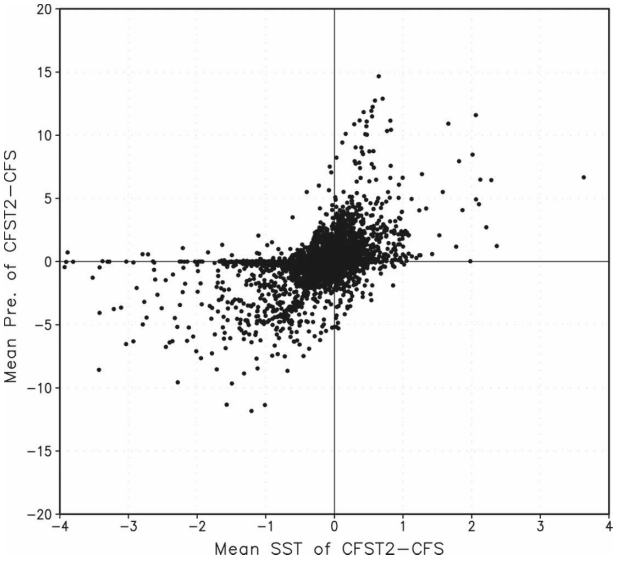

FIG. 3. Scatterplot between the DJF seasonal-mean coupled model hindcast SST bias (*x* axis) and tier-two minus coupled hindcast DJF seasonal mean rainfall climatology (*y* axis). The scatterplot is for all oceanic grid points between 20°S and 20°N. The spatial plot of SST bias is shown in Fig. 1, and the difference in rainfall climatology between the two hindcasts is shown in Fig. 2 (bottom).

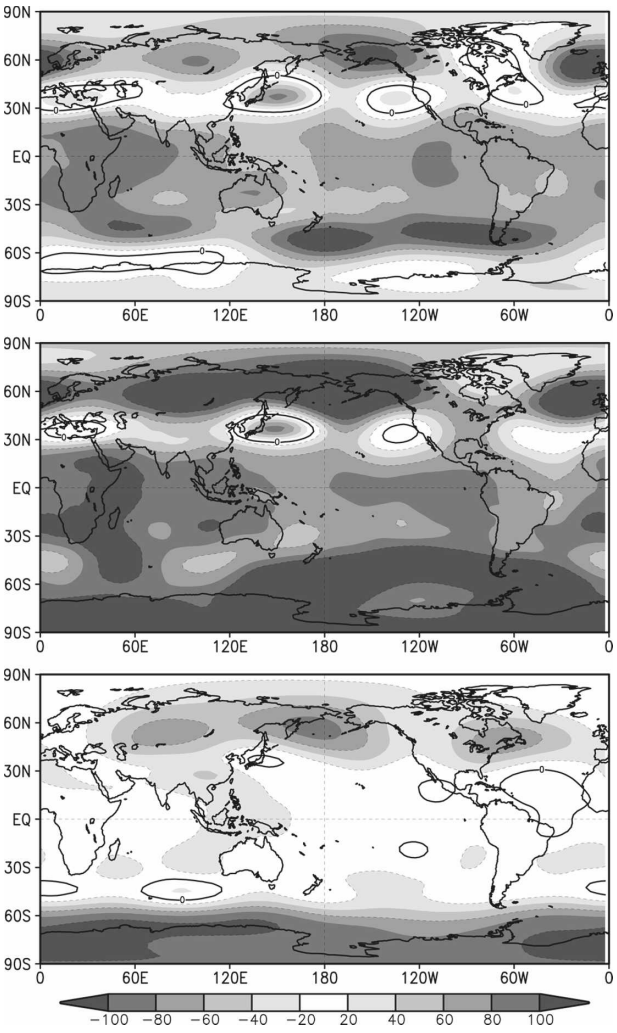

FIG. 4. Model minus observed DJF seasonal-mean 200-mb height climatology for the (top) coupled model and (middle) tier-two hindcast. (bottom) The tier-two minus coupled hindcast 200-mb height climatology for DJF seasonal mean. Climatology was computed based on the 1982–2005 period, and a 15-member ensemble mean was used for the model. Units are meters; the zero contour is plotted.

SSTs; one exception is that the enhanced mean rainfall for the tier-two hindcasts east of 120°E–120°W is collocated with the colder mean state for SST. This is possibly due to a large reduction in mean rainfall over the Maritime Continent and associated changes in the vertical circulation. Such "nonlocal" differences in the rainfall that are not directly linked to the underlying SSTs are expected because of mass continuity across pressure surface; that is, changes in vertical velocity at one location need to be compensated by changes elsewhere (Kumar et al. 2004; Neelin et al. 2006).

Shown in Fig. 4 is the bias for the 200-mb heights for the CFS and the tier-two hindcasts. Mean bias for both sets of hindcasts is toward lower heights, with the bias for the tier-two hindcasts (Fig. 4, middle panel) being larger than the bias in the coupled run (Fig. 4, top panel). Increased bias for the 200-mb heights (or lowering of heights in the tier-two hindcasts; Fig. 3, bottom panel) is physically consistent with the removal of the warm SST bias from the CFS hindcasts (see Fig. 1). In other words, although the height bias in the CFS hindcasts is smaller, it is likely an artifact of a generally warm SST bias leading to higher 200-mb heights. Apart from a general increase in the height bias for tier-two hindcasts, the spatial structure of the height bias is very similar, and is further quantified from the analysis of the eddy heights shown in Fig. 5 where the biases for eddy heights between two hindcasts also have a remarkably similar spatial structure, with spatial correlation of 0.85. The difference in the CFS and tier-two heights (Fig. 5, bottom panel) has a hint of a wave train that emanates over the Maritime Continent and propagates eastward in the extratropical latitudes. The sign of this wave train feature is consistent with the lower rainfall in the tier-two hindcasts in that lower heights are collocated with lower rainfall over the Maritime Continent.

To summarize, the overall features of rainfall and 200-mb height bias between CFS and tier-two hindcasts have similar features, and at the same time differences are physically consistent with the bias correction ap-

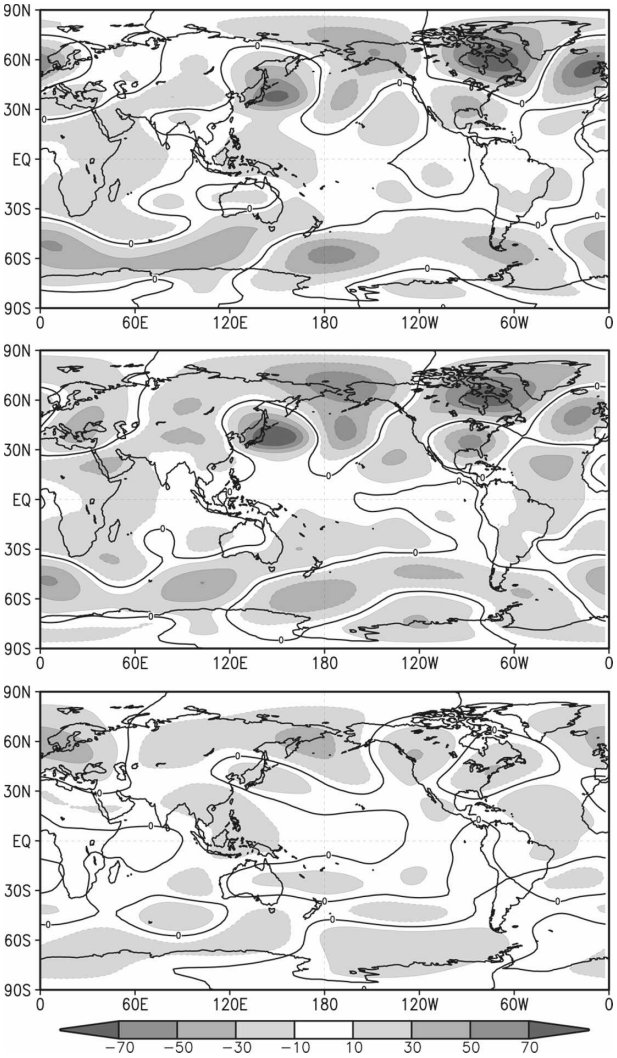

FIG. 5. As in Fig. 4 but for the 200-mb eddy heights.

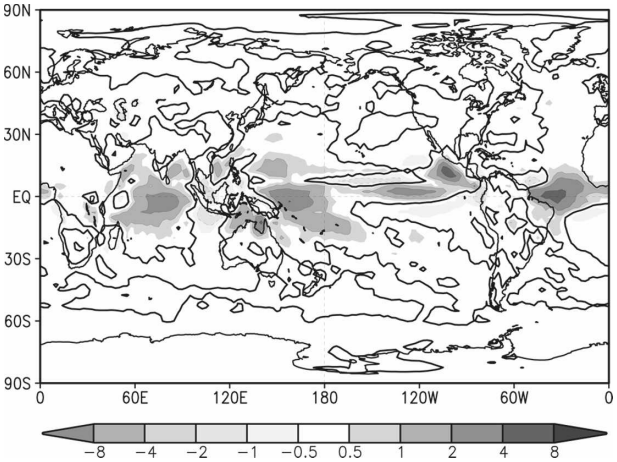

FIG. 6. Difference in DJF seasonal-mean rainfall variability related to SSTs. SST-forced variability is defined as the standard deviation of ensemble mean rainfall anomalies computed based on the 1982–2005 period. Change in SST-forced variability is shown as the difference in standard deviation of ensemble means for the tier-two minus coupled hindcasts. Units are mm day^{-1}; zero contour is plotted.

plied to SSTs prior to their specification in the tier-two hindcasts.

b. *Analysis of differences in the interannual variability*

In this subsection, interannual variability of rainfall and 200-mb height is analyzed. The main focus is on the seasonal mean variability related to SSTs (the so-called external variance of seasonal means) based on the ensemble mean hindcast anomalies. Computation of the external and internal variance follows the standard procedure well documented in the literature (see, e.g., Kumar and Hoerling 1995; Rowell et al. 1995).

The change in the interannual variability of rainfall related to the SSTs is shown is Fig. 6. For the sake of comparison with the change in mean rainfall (Fig. 4, bottom panel), the change in the interannual variability of the rainfall related to SSTs is shown as a difference in standard deviation. Differences in the external variability in rainfall are confined to the deep tropics where external variability for rainfall is largest (Peng et al. 2000). Similar to the spatial structure of changes in the mean rainfall, the spatial structure of change in the external variability can be attributed to the difference in the SST bias (Fig. 1). For example, increased external variability for the tier-two hindcasts is found over the equatorial Atlantic, equatorial tropical eastern Pacific, and the equatorial Indian Ocean—regions in which mean SSTs for the tier-two hindcasts are also warmer. Similarly, a reduction in external variability of rainfall is found over the Maritime Continent.

A general correspondence between the sign of change in the external variability of rainfall and the sign of SST bias can be physically interpreted based on the nonlinear dependence of rainfall on SSTs and that, on the lower side, rainfall is bounded by zero (Hoerling et al. 1997; Hoerling et al. 2001). For the regions where mean SST for the tier-two hindcasts is warmer (cooler) than the coupled hindcasts, interannual variability in SSTs can also generate larger (smaller) swings in rainfall anomalies, leading to a larger (smaller) amplitude for the SST-related interannual variability in rainfall. This mechanism is similar to the scatterplot in Fig. 3 (upper-right quadrangle) where increasingly warmer mean SSTs result in progressively larger positive mean rainfall anomalies, whereas increasingly colder mean SST anomalies (lower-left quadrangle) do not lead to increasingly large negative rainfall anomalies.

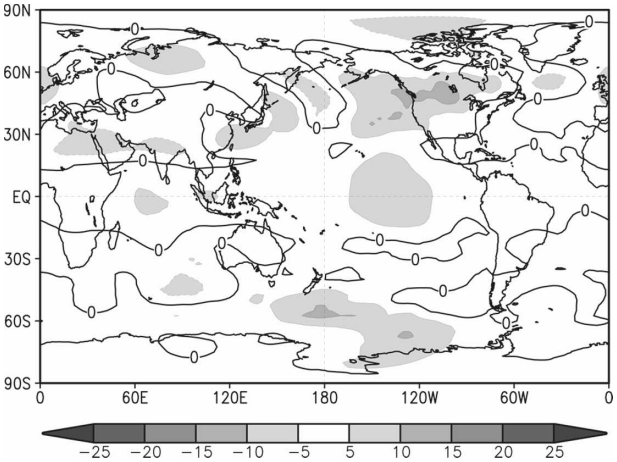

FIG. 7. As in Fig. 7 but for 200-mb heights.

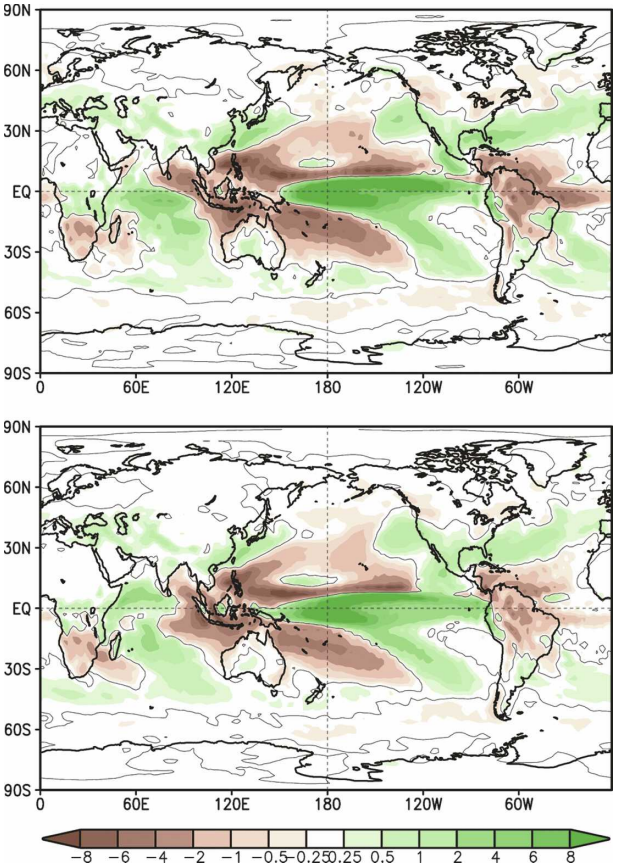

FIG. 8. DJF seasonal-mean rainfall composite for the (top) tier-two and (bottom) coupled hindcast. Composite is shown as the difference between the warm and cold composite, a procedure that enhances the linear signal related to SSTs. Years for the composite are chosen based on DJF Niño-3.4 SST index being above/below one standard deviation. Based on this criterion, the warm ENSO years are 1983, 1987, 1992, 1998, 2003, and the cold ENSO years are 1985, 1989, 1996, 1999, 2000. Units are mm day^{-1}; zero contour is plotted.

An increase in the SST-related interannual variability of rainfall for the tier-two hindcasts has some bearing on the corresponding SST-forced variability for the 200-mb heights shown in Fig. 7. The external variability of 200-mb heights for the tier-two hindcast is larger in tropical latitudes, particularly east of the date line. In the Western Hemisphere, larger values are also located in the extratropical latitudes, and symmetry around the equator suggests a tropical origin for this increase. Indeed, this increase in the SST-forced variance for the 200-mb heights can be attributed to the increased SST-forced tropical rainfall variance leading to an amplified wavelike pattern of external height variance emanating from the tropical latitudes in the eastern Pacific. In the discussion below, this would be further substantiated from the analysis of the atmospheric response to El Niño–Southern Oscillation (ENSO) SST variability. Another feature in Fig. 7 to note is that change in the external variability of height is stronger in the Northern Hemisphere and is expected from the seasonal characteristics of the tropical–extratropical interactions (Livezey et al. 1997; Kumar et al. 2003).

As part of the SST-related interannual variability of the atmospheric anomalies, the atmospheric response to ENSO SSTs is analyzed next. As was discussed in section 1, a motivation for this study was to assess the scope of errors in our understanding of the global atmospheric influence of tropical SSTs that, in the past, has extensively relied upon tier-two AGCM experiments. A comparison of the same response between two hindcasts would provide an assessment of possible errors in the atmospheric response to tropical SSTs (and particularly those related to ENSO SSTs) due to the misrepresentation of coupled ocean–atmosphere evolution in the tier-two experimental setup.

A comparison of the atmospheric response to the dominant mode of tropical SST variability, that is, ENSO SSTs, can be done in several ways. Our approach follows the composite technique and results following this approach are compared in Figs. 8 and 9. The composites are shown as the difference between the warm and cold composites, a procedure that enhances the linear component of the atmospheric response to SSTs (Hoerling et al. 1997). Since the composites are based on ensemble means, the spatial structures of the composite anomalies are highly significant.

For both sets of hindcasts, the spatial pattern of the rainfall composite has the familiar structure with an increase of rainfall anomalies east of the date line in the tropical equatorial latitude surrounded by a horseshoe-like pattern of negative rainfall anomalies (Hoerling and Kumar 2002; Peng et al. 2000). Indicating a high

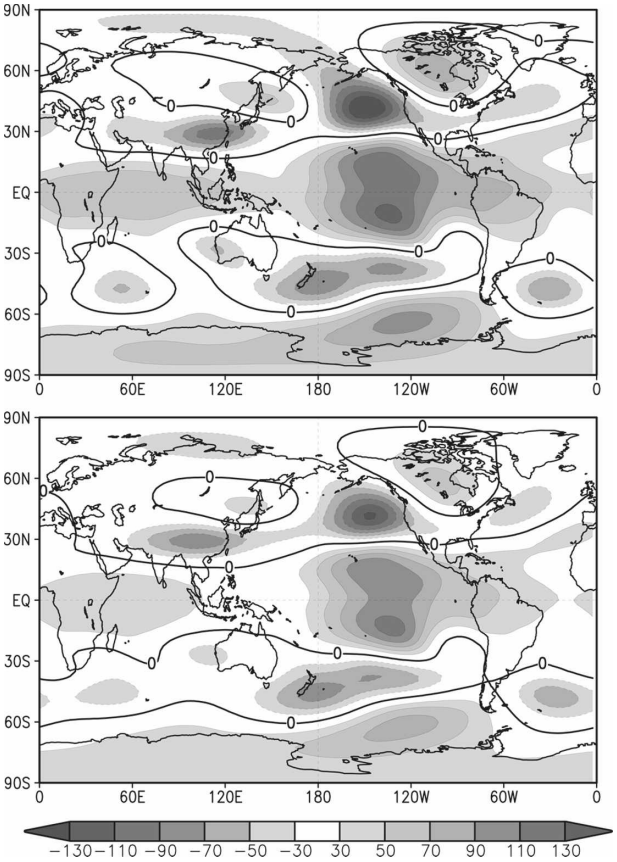

FIG. 9. As in Fig. 8 but for 200-mb heights. Units are meters.

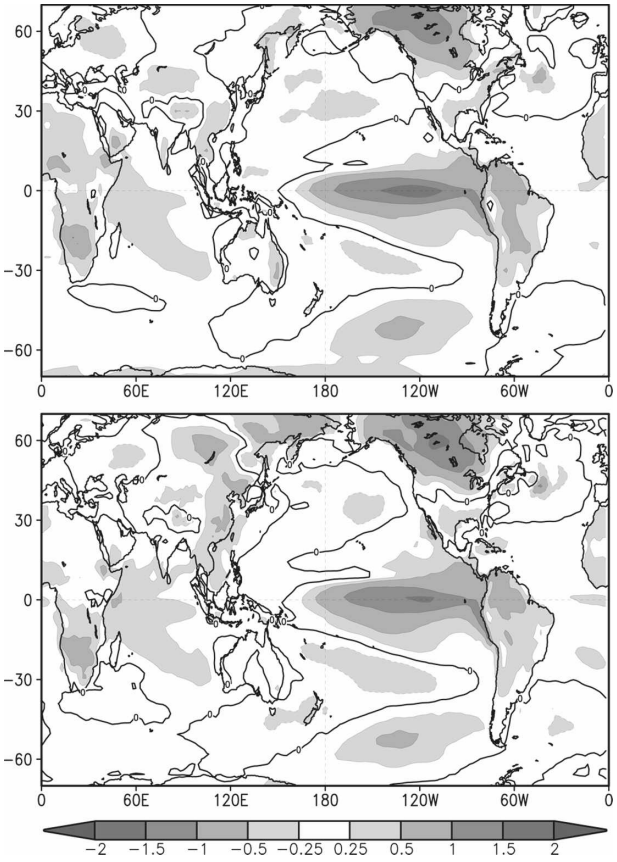

FIG. 10. Spatial structure of SSTs related to the dominant pattern of the 200-mb ensemble-mean height variability for the (top) tier-two and (bottom) coupled hindcast. Dominant pattern of height variability is obtained based on EOF analysis, and the corresponding SST pattern is obtained by regressing time series of the dominant height EOF with SSTs. EOF analysis for heights was for DJF ensemble mean heights for the 1982–2005 period. Units are in °C.

degree of spatial resemblance, the spatial correlation between the tier-two and coupled hindcast rainfall composites is 0.90. The amplitude of rainfall response to ENSO SSTs is larger in the tier-two runs and is consistent with the discussion of an increase in SST-forced rainfall variability in Fig. 6.

An analysis similar to the rainfall, but for 200-mb heights, is shown in Fig. 9. Once again, the spatial pattern of the atmospheric response for both sets of hindcasts is represented by the well-documented pattern of the atmospheric response to ENSO SSTs (Hoerling and Kumar 2002; Peng et al. 2000). The largest response in tropical latitudes is confined to the eastern equatorial Pacific with a wave train response extending into the extratropical latitudes in both hemispheres. The spatial correlation between the two responses in Fig. 9 is 0.98, indicating a high degree of spatial resemblance. Similar to the rainfall, the amplitude of the 200-mb height response is stronger for the tier-two hindcasts and is consistent with the analysis of SST-forced height variability in Fig. 7

To infer the influence of tropical SSTs on the atmospheric response, we also analyzed the dominant mode of the ensemble-mean global 200-mb heights based on the empirical orthogonal function technique. To infer the forcing mechanism responsible for this mode, we regressed the principle component time series of the dominant mode of height variability with global SSTs. The spatial patterns of global SSTs obtained based on this analysis are shown in Fig. 10 for the tier-two and the coupled hindcasts and, as expected, correspond to the spatial pattern of ENSO SST variability. The spatial correlation between the two patterns is 0.9 and, once again, implies a SST forcing pattern that is very similar between tier-two and coupled hindcasts.

c. A comparison of prediction skill of coupled and tier-two forecasts

A more stringent test of assessment of interannual variability between the two sets of hindcasts is done

based on their comparison of the observed variability. As the observed seasonal means are a manifestation of coupled variability, it is feasible that the observed variability may relate better to the coupled hindcasts than to the tier-two hindcasts. This comparison is quantified via the anomaly correlations between the observed and hindcast anomalies.

Prior to comparing the anomaly correlation based on two sets of hindcasts and the observations, anomaly correlations of the ensemble mean interannual variability between two sets of hindcasts themselves is first analyzed. This analysis illustrates to what extent the ensemble mean atmospheric variability between tier-two and coupled hindcasts has similar time evolution. Furthermore, this analysis also complements the analysis of SST-forced interannual variability, discussed in section 3c.

The spatial pattern of temporal anomaly correlation between the two sets of hindcasts for rainfall and 200-mb height is shown in Fig. 11. The anomaly correlations are based on the 1982–2005 period and are for the ensemble-mean hindcast anomalies.

For rainfall, the largest anomaly correlations between two hindcasts are in the equatorial tropical eastern Pacific. This spatial pattern of SST-forced rainfall covariability between the two hindcasts can be explained using signal-to-noise considerations. Regions where the SST-forced atmospheric signal dominates compared to the internal variability of the atmospheric seasonal means (i.e., large signal-to-noise ratio), the interannual variability between the two simulations correlates well. Regions where the internal variability of seasonal mean dominates (i.e., small signal-to-noise ratio), and may not be effectively filtered out based on an ensemble size of 15, correlation between the two sets of hindcasts is low. To confirm this, a contour that highlights the average signal-to-noise ratio of 0.4 (with signal-to-noise ratio defined as the ratio of external versus the internal variability) is also shown in Fig. 11. In general, areas with large anomaly correlations are confined within this particular contour.

A similar analysis is repeated for 200-mb heights (Fig. 11, bottom panel). The spatial pattern of the anomaly correlation for 200 mb is much smoother, and regions with high correlation have a much wider areal extent. For example, correlations exceeding 0.9 are found throughout the tropical belt, indicating a strong degree of temporal phase relationship between the two hindcasts. This, once again, is a consequence of the spatial structure of signal-to-noise ratio for the interannual variability of height (see, e.g., Peng et al. 2000). Also included in the spatial map is the contour for which signal-to-noise ratio for seasonal mean heights is 0.4, and regions with large anomaly correlations are generally confined within this contour.

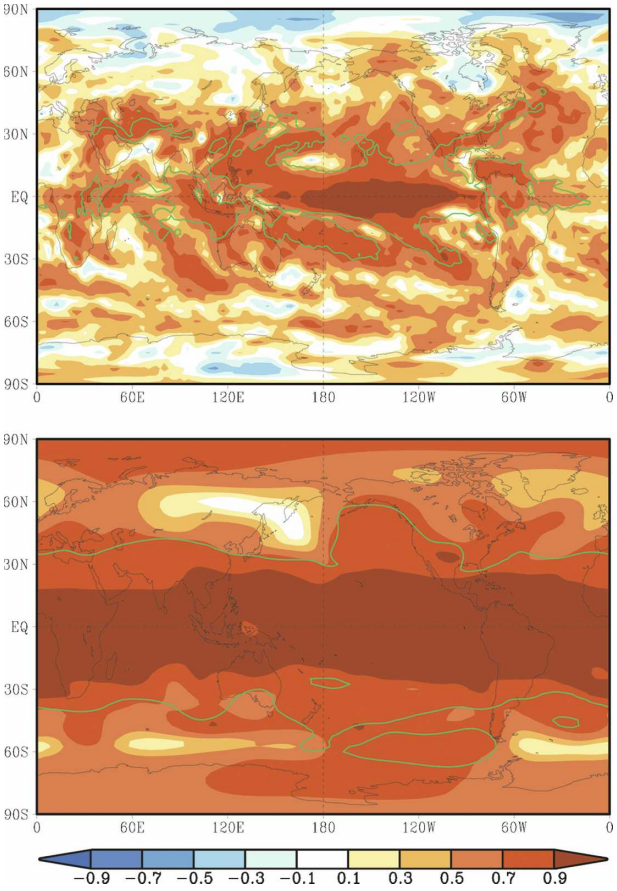

FIG. 11. Spatial pattern of temporal anomaly correlation between tier-two and coupled hindcast ensemble mean anomalies for (top) rainfall and (bottom) 200-mb heights. Anomaly correlation is based on DJF seasonal mean over the 1982–2005 period. The contour corresponds to the signal-to-noise ratio of 0.4, where signal-to-noise ratio is defined as the ratio of external-to-total variance of DJF seasonal means. The signal-to-noise ratio within the contour exceeds 0.4.

The final analysis is a comparison of prediction skill of the two hindcasts, quantified as the anomaly correlation between the ensemble mean hindcast anomaly and the observed anomaly. The prediction skill for rainfall and 200-mb height is shown in Fig. 12.

Consistent with regions where the signal-to-noise ratio is large in Fig. 11, and also consistent with the ENSO composite in Fig. 8, the regions of high predictive skill are located in the equatorial tropical eastern Pacific. This spatial structure of rainfall skill is consistent with earlier studies (e.g., Peng et al. 2000). There are very few geographical regions where the difference in predictive skill for rainfall between tier-two and coupled hindcasts is significantly different from zero at the 95% confidence level.

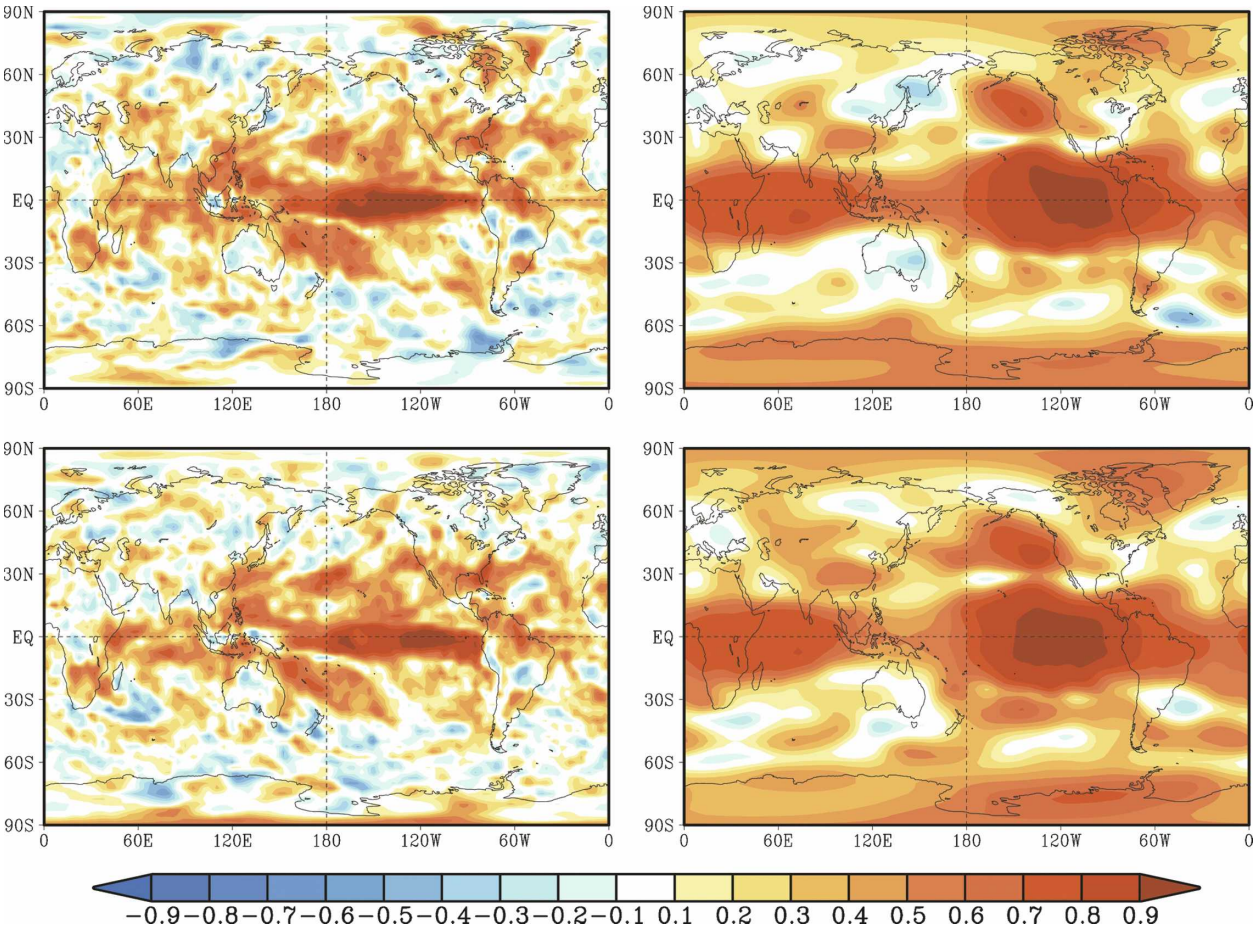

FIG. 12. Spatial pattern of (left) rainfall and (right) 200-mb height temporal anomaly correlation between (top) tier-two hindcast and observations and (bottom) coupled hindcast and observations. Anomaly correlations are for DJF seasonal mean over the 1982–2005 period, and hindcast anomalies are the DJF ensemble means.

The spatial structure of predictive skill for 200-mb heights for the two hindcasts is also similar to that documented in previous studies (Peng et al. 2000) and corresponds to the atmospheric response pattern of ENSO SSTs (see Fig. 9). High anomaly correlations are located in the tropical eastern Pacific, and, similar to the composite 200-mb height response in Fig. 9, regions of high correlation also extend into extratropical latitudes.

Differences in predictive skill are further quantified in Fig. 13 in which the percentage of grid points exceeding a particular numerical value of correlation is shown. This comparison is for rainfall (Fig. 13, upper panel) and 200-mb height (Fig. 13, lower panel). For both, and for high skill regimes, for example, anomaly correlation exceeding 0.6, the percentage of grid points for tier-two and coupled hindcasts is almost equal. It is for 200-mb heights and for small correlation regimes between 0 and 0.5 that coupled hindcasts have an advantage over the tier-two hindcasts. Similarity of the high correlation regime is easy to explain. Regions with large skill, particularly for the interannual variability of rainfall, exist over oceanic regions where the ocean is the driving force for the atmospheric variability. As long as the time history of SSTs is given, a strong atmospheric response to SSTs is a sufficient condition so that the simulation of atmospheric interannual variability in the uncoupled simulations is the same as in the coupled simulations.

A plausible explanation for improvements for the low skill regimes is that it is a manifestation of coupled ocean–atmosphere evolution in the coupled simulations. There are indications that, for the AGCM-alone simulations, SST and rainfall covariability in oceanic regions (away from the equatorial tropical eastern Pacific) tends to be more positive compared to that in the coupled simulations (Kumar and Hoerling 1998; Wu et al. 2006). Furthermore, such differences only occur over low SST–rainfall correlation regimes and over the

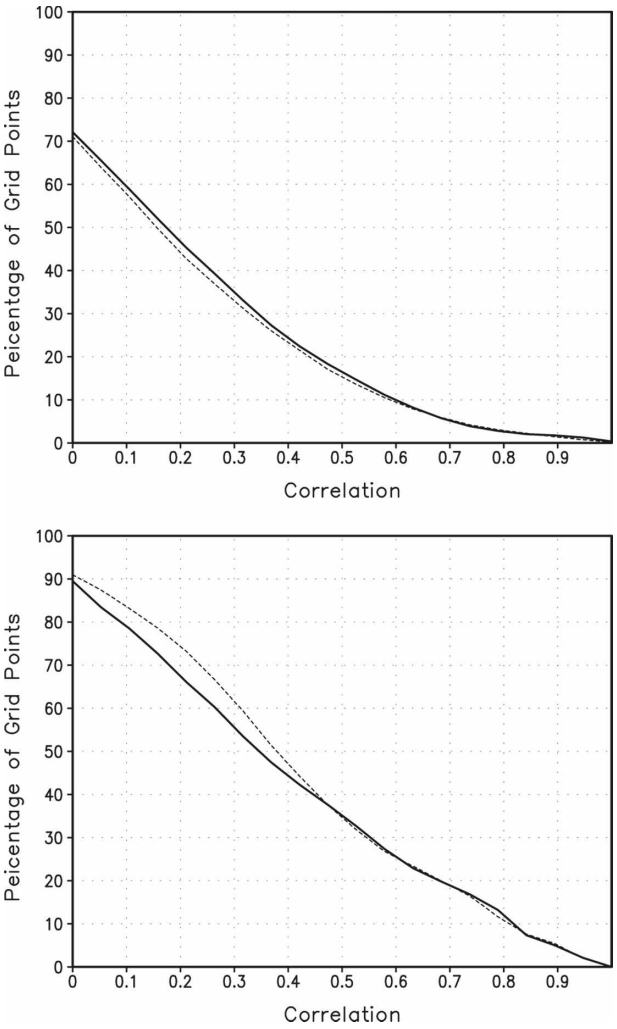

FIG. 13. Percentage of grid points (y axis) that exceed a particular value of anomaly correlation (x axis) for (top) rainfall and (bottom) 200-mb heights. Percentages are not plotted for the negative correlations. The dash line is for the coupled CFS hindcasts, and the black line is for the tier-two hindcasts. Cosine weighting of grid points is included in the evaluation of percentage.

oceanic regions where the atmosphere tends to force the ocean.

The SST–rainfall relationship on shorter time scales depends on the phase relationship between atmospheric and oceanic variability and is better simulated in coupled integrations leading to (documented) improvements in the simulation characteristics of various atmospheric phenomena, for example, MJO characteristics (Sperber 2004; Fu and Wang 2004). The SST–rainfall covariability for the seasonal time scale analyzed here is the rectified influence of ocean–atmosphere coupled variability on the short time scale. It is feasible that this covariability is misrepresented in AGCM-alone simulations, leading to stronger control of SSTs on the rainfall anomalies, and can explain degradation of 200-mb skill for AMIP hindcasts for low correlation regimes. Another possibility for differences in the correlation is the change in the mean state between coupled and tier-two simulations; differences that can influence the interannual atmospheric variability to further augment the influence of coupled ocean–atmosphere evolution.

d. An analysis for JJAS seasonal mean

Although the results for the winter season indicate that the evolution on the atmospheric variability is similar in two hindcasts, in a series of recent papers a possibility has been raised that the same conclusion may not hold during summer, particularly for the interannual variability of summer monsoon over Southeast Asia (Wang et al. 2005; Krishna Kumar et al. 2005). A possible physical reason for different behavior is that, during the boreal winter, ocean dynamics related to ENSO dominates the temporal evolution of SSTs in the equatorial tropical Pacific, and this variability in turn dominates the interannual atmospheric variability over the globe. With the lack of dominance of ENSO variability during boreal summer, the coupled ocean–atmospheric evolution may have a larger impact on the interannual variability of the atmospheric circulation.

Following previous studies (Wang et al. 2005; Krishna Kumar et al. 2005), the analysis of variability of summer circulation focuses on the Indian monsoon rainfall (IMR) during the JJAS season. Two separate assessments of IMR are presented here. Figure 14 shows a comparison of time series of rainfall area averaged over the IMR between observations versus coupled and tier-two hindcasts. The interannual variability of the coupled CFS hindcast (short-dash line) has a better in-phase relationship with the observations (black curve) compared to the interannual variability of the tier-two hindcasts (long-dash line). Indeed, the correlation between the CFS and the observed time series is 0.49 and compares favorably against the correlation of -0.26 for the tier-two hindcasts. This difference in correlation is similar to one reported by Krishna Kumar et al. (2005) where several AMIP and coupled simulations were analyzed.

The second analysis presented here is the simultaneous correlation between the IMR and the interannual SST variability over the globe (Fig. 15). For the observations, interannual variability of the IMR rainfall has a weak negative correlation with SSTs in the equatorial tropical eastern Pacific SSTs. A similar correlation is also found for the coupled CFS hindcast. On the other hand, for the tier-two hindcasts, the correlation of

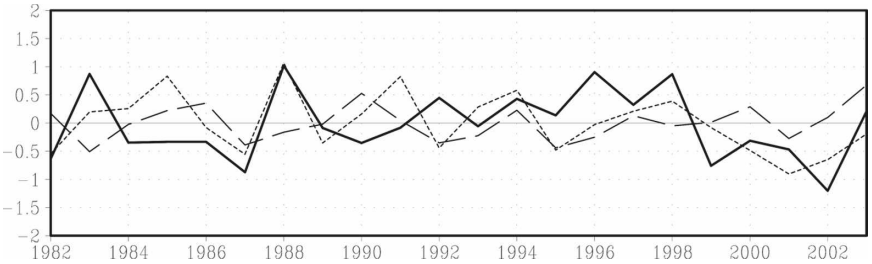

FIG. 14. Time series of JJAS area-averaged Indian monsoon rainfall for observations (black curve), coupled CFS hindcasts (short-dash line), and tier-two hindcasts (long-dash line). Area average is over the spatial domain 5°–30°N, 60°–90°E. Units are mm day^{-1}.

the IMR with SSTs in the equatorial tropical eastern Pacific is weakly positive (see Krishna Kumar et al. 2005).

e. An alternative interpretation of the comparison of skill

As discussed in section 2, the primary goal of the tier-two hindcast runs is to assess improvement in seasonal prediction skill due to SST bias correction. Our analysis indicates that, for the CFS, a posteriori removal of SST bias does not lead to improved seasonal forecasts based on tier-two predictions. This is to be expected because, for the CFS, biases in the tropical SSTs are generally less than 0.5 and are not large enough to have a substantial influence on atmospheric interannual variability. On the other hand, for longer lead forecasts when tropical SST biases are larger (e.g., March–May predictions from October initial conditions), there are indications that forecasts based on the two-tier prediction system do tend to improve seasonal prediction skill (results not shown).

4. Summary and concluding remarks

In this paper, differences in atmospheric mean and its interannual variability between two sets of hindcasts were analyzed. The interannual variability of SSTs between the two sets of hindcasts was the same, while their mean states were different. The purpose of the study was to analyze how much the lack of a coupled ocean–atmosphere evolution influences the atmospheric mean state and its interannual variability in the atmospheric-alone AGCM simulations.

The main focus of the analysis was on the DJF seasonal mean rainfall and 200-mb heights. The former was chosen because the interannual variability of SSTs has a direct consequence on rainfall variability (particularly in the tropical latitudes), while the latter was selected based on the fact that, for this field, global con-

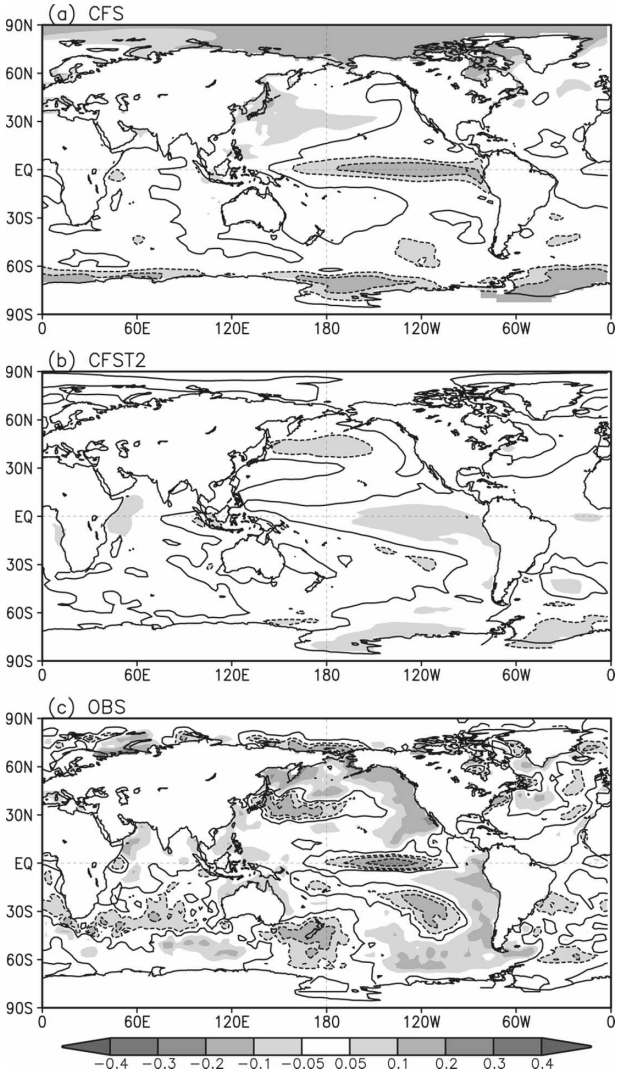

FIG. 15. Spatial map of temporal correlation between the IMR and SST variability over the globe for (top) coupled CFS and (middle) tier-two hindcasts and (bottom) observations. The time series of IMR is shown in Fig. 14.

sequences of ENSO SST variability has a clear manifestation. For both variables, the analysis indicates that differences in the means between two hindcasts could be related to the corresponding differences in the mean SST state. A similar conclusion can also be made for the SST-forced atmospheric variability between two sets of hindcasts. Indeed, for high skill regimes an analysis of the skill of the two hindcasts demonstrated small differences in hindcast skill.

The analysis (and its conclusions) discussed here can also be interpreted in the context of the influence of coupled ocean–atmosphere evolution in extratropical oceans. Our discussion mostly focused on the atmospheric variability within the premise of tropical SST variability. Many studies have also investigated the role of coupled ocean–atmosphere evolution in the extratropical oceans on atmospheric variability (Gallimore 1995; Delworth 1996; Bladé 1997; Barsugli and Battisti 1998). In the extratropical oceans there is a strong theoretical basis for understanding the influence of the coupled ocean–atmosphere evolution on atmospheric variability, that is, the thermal damping mechanism that can influence atmosphere variability (Barsugli and Battisti 1998). In general, these studies have shown small influence on seasonal atmospheric variability. The analysis presented here also leads to the same conclusion about the influence of the extratropical coupled ocean–atmosphere evolution on atmospheric variability.

Although the analysis of the boreal winter seasonal means presented here demonstrates little influence of coupled ocean–atmosphere evolution, it is not to say that this is true for all time scales or for different seasons. For example, it has been demonstrated that, for correct simulation of MJO variability, coupled ocean–atmosphere evolution may be important (Sperber 2004; Fu and Wang 2004; Seo et al. 2007). On the other hand, how much this influence on high-frequency variability rectifies the variability of seasonal means also needs to be quantified. It is also possible that, even for seasonal means, the coupled ocean–atmosphere evolution may be of importance for some specific phenomenon or for some other season. Indeed, an analysis of the interannual IMR variability confirmed recent results that the simulation of the IMR is better represented in the coupled model simulations (e.g., Wang et al. 2005; Krishna Kumar et al. 2005).

To build confidence in the conclusions presented here and to further quantify the role of coupled ocean–atmosphere evolution on the atmospheric variability, a similar analysis needs to be conducted with other AGCMs, particularly using an experimental setup where the SST in the tier-two and coupled hindcasts (or simulations) is identical.

As we mentioned in section 1, the purpose of this analysis is to assess what the level of error is due to approximating a physical reality in the tier-two (or the AMIP) simulations. A similar kind of error analysis is routinely done when various approximations are applied in any physical theory. Some investigations may have compelling reasons for using AMIP integrations. One such example includes the attribution of observed atmospheric interannual variability to the observed SST anomalies, an exercise that by design relies on AMIP simulations forced with observed SST anomalies. For proper interpretation of such applications, an estimate of error associated with an AMIP-type experimental setup needs to be documented.

Acknowledgments. KHS was funded by Korea Meteorological Administration Research and Development Program under Grant CATER 2007-4208. Constructive comments from three anonymous reviewers and from Drs. Song Yang and Yan Xue are gratefully acknowledged.

REFERENCES

Annamalai, H., P. Liu, and S.-P. Xie, 2005: Southwest Indian Ocean SST variability: Its local effect and remote influence on Asian monsoons. *J. Climate,* **18,** 4150–4167.

Barsugli, J. J., and D. S. Battisti, 1998: The basic effects of atmosphere–ocean thermal coupling on midlatitude variability. *J. Atmos. Sci.,* **55,** 477–493.

Bengtsson, L., U. Schlese, E. Roeckner, M. Latif, T. P. Barnett, and N. E. Graham, 1993: A two-tiered approach to long-range climate forecasting. *Science,* **261,** 1026–1029.

Biasutti, M., A. H. Sobel, and Y. Kushnir, 2006: AGCM precipitation biases in the tropical Atlantic. *J. Climate,* **19,** 935–958.

Bladé, I., 1997: The influence of midlatitude ocean–atmosphere coupling on the low-frequency variability of a GCM. Part I: No tropical SST forcing. *J. Climate,* **10,** 2087–2106.

Bretherton, C. S., and D. S. Battisti, 2000: An interpretation of the results from atmospheric general circulation models forced by the time history of the observed sea surface temperature distribution. *Geophys. Res. Lett.,* **27,** 767–770.

Delworth, T. L., 1996: North Atlantic interannual variability in a coupled ocean–atmosphere model. *J. Climate,* **9,** 2356–2375.

Fu, X., and B. Wang, 2004: The boreal-summer intraseasonal oscillations simulated in a hybrid coupled atmosphere–ocean model. *Mon. Wea. Rev.,* **132,** 2628–2649.

Gallimore, R. G., 1995: Simulated ocean–atmosphere interaction in the North Pacific from a GCM coupled to a constant-depth mixed layer. *J. Climate,* **8,** 1721–1737.

Gates, W. L., 1992: AMIP: The Atmospheric Model Intercomparison Project. *Bull. Amer. Meteor. Soc.,* **73,** 1962–1970.

Hoerling, M. P., and A. Kumar, 2002: Atmospheric response patterns associated with tropical forcing. *J. Climate,* **15,** 2184–2203.

——, ——, and M. Zhong, 1997: El Niño, La Niña, and the nonlinearity of their teleconnections. *J. Climate,* **10,** 1769–1786.

——, ——, and T. Xu, 2001: Robustness of the nonlinear climate response to ENSO's extreme phases. *J. Climate,* **14,** 1277–1293.

Janowiak, J. E., and P. Xie, 1999: CAMS–OPI: A global satellite–rain gauge merged product for real-time precipitation monitoring applications. *J. Climate,* **12,** 3335–3342.

Ji, M., A. Kumar, and A. Leetmaa, 1994: A multiseason climate forecast system at the National Meteorological Center. *Bull. Amer. Meteor. Soc.,* **75,** 569–577.

Kharin, V. V., F. W. Zwiers, and X. Zhang, 2005: Intercomparison of near-surface temperature and precipitation extremes in AMIP-2 simulations, reanalyses, and observations. *J. Climate,* **18,** 5201–5223.

Krishna Kumar, K., M. P. Hoerling, and B. Rajagopalan, 2005: Advancing dynamical prediction of Indian monsoon rainfall. *Geophys. Res. Lett.,* **32,** L08704, doi:10.1029/2004GL021979.

Kumar, A., and M. P. Hoerling, 1995: Prospects and limitations of seasonal atmospheric GCM predictions. *Bull. Amer. Meteor. Soc.,* **76,** 335–345.

——, and ——, 1998: Specification of regional sea surface temperatures in atmospheric general circulation model simulations. *J. Geophys. Res.,* **103,** 8901–8907.

——, S. Schubert, and M. Suarez, 2003: Variability and predictability of 200-mb seasonal mean heights during summer and winter. *J. Geophys. Res.,* **108,** 4169, doi:10.1029/2002JD002728.

——, F. Yang, L. Goddard, and S. Schubert, 2004: Differing trends in the tropical surface temperatures and precipitation over land and oceans. *J. Climate,* **17,** 653–664.

Lau, N.-C., 1997: Interactions between global SST anomalies and midlatitude atmospheric circulation. *Bull. Amer. Meteor. Soc.,* **78,** 21–33.

Livezey, R. E., M. Masutani, A. Leetmaa, H. Rui, M. Ji, and A. Kumar, 1997: Teleconnective response of the Pacific–North American region atmosphere to large central equatorial Pacific SST anomalies. *J. Climate,* **10,** 1787–1820.

Nakaegawa, T., and M. Kanamitsu, 2006: Cluster analysis of the seasonal forecast skill of the NCEP SFM over the Pacific–North America sector. *J. Climate,* **19,** 123–138.

Neelin, J. D., M. Münnich, H. Su, J. E. Meyerson, and C. E. Holloway, 2006: Tropical drying trends in global warming models and observations. *Proc. Natl. Acad. Sci. USA,* **103,** 6110–6115.

Nigam, S., and A. Ruiz-Barradas, 2006: Seasonal hydroclimate variability over North America in global and regional reanalyses and AMIP simulations: Varied representation. *J. Climate,* **19,** 815–837.

Peng, P., A. Kumar, A. G. Barnston, and L. Goddard, 2000: Simulation skills of the SST-forced global climate variability of the NCEP–MRF9 and Scripps–MPI ECHAM3 models. *J. Climate,* **13,** 3657–3679.

Rowell, D., C. Folland, K. Maskell, and M. Ward, 1995: Variability of summer rainfall over tropical north Africa (1906–92): Observations and modelling. *Quart. J. Roy. Meteor. Soc.,* **121,** 669–704.

Saha, S., and Coauthors, 2006: The NCEP Climate Forecast System. *J. Climate,* **19,** 3483–3517.

Seo, K.-H., J.-K. E. Schemm, W. Wang, and A. Kumar, 2007: The boreal summer intraseasonal oscillation simulated in the NCEP Climate Forecast System: The effect of sea surface temperature. *Mon. Wea. Rev.,* **135,** 1807–1827.

Sperber, K. R., 2004: Madden–Julian variability in NCAR CAM2.0 and CCSM2.0. *Climate Dyn.,* **23,** 259–278.

Trenberth, K. E., G. W. Branstator, D. Karoly, A. Kumar, N.-C. Lau, and C. Ropelewski, 1998: Progress during TOGA in understanding and modeling global teleconnections associated with tropical sea surface temperatures. *J. Geophys. Res.,* **103** (C7), 14 291–14 324.

Wang, B., Q. Ding, X. Fu, I.-S. Kang, K. Jin, J. Shukla, and F. Doblas-Reyes, 2005: Fundamental challenge in simulation and prediction of summer monsoon rainfall. *Geophys. Res. Lett.,* **32,** L15711, doi:10.1029/2005GL022734.

Wang, W., S. Saha, H.-L. Pan, S. Nadiga, and G. White, 2005: Simulation of ENSO in the new NCEP Coupled Forecast System Model (CFS03). *Mon. Wea. Rev.,* **133,** 1574–1593.

Wu, R., B. P. Kirtman, and K. Pegion, 2006: Local air–sea relationship in observations and model simulations. *J. Climate,* **19,** 4914–4932.